

A Neural-Network-Based Approach for Loose-Fitting Clothing

YONGXU JIN, Stanford University, USA and Epic Games, USA

DALTON OMENS, Stanford University, USA and Epic Games, USA

ZHENGLIN GENG, Epic Games, USA

JOSEPH TERAN, University of California, Davis, USA and Epic Games, USA

ABISHEK KUMAR, Sony Corporation of America, R&D US Laboratory, USA

KENJI TASHIRO, Sony Corporation of America, R&D US Laboratory, USA

RONALD FEDKIW, Stanford University, USA and Epic Games, USA

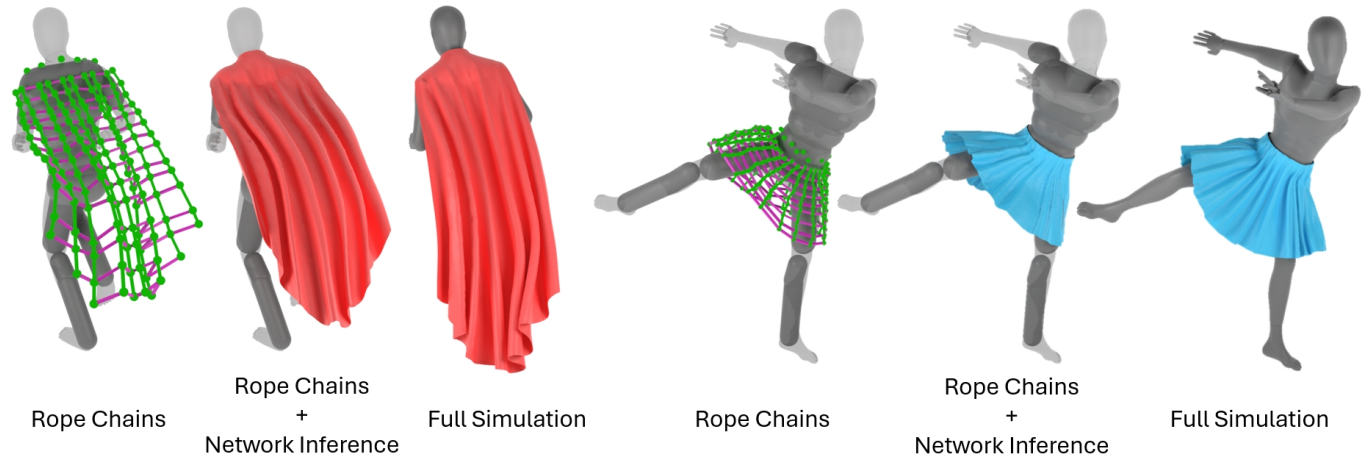


Fig. 1. We introduce a rope chain simulation approach to efficiently model cloth dynamics using a small number of degrees of freedom. Analytic signed distance functions are used to efficiently manage collisions with the body mesh. Neural networks are utilized to skin a mesh from the simulated degrees of freedom and to capture the detailed mesh shapes. Our results (the second and fifth images) not only produce dynamics similar to full numerical simulations (the third and sixth images) but also do not suffer from the locking and/or overstretching typical of real-time physics-based simulations.

Since loose-fitting clothing contains dynamic modes that have proven to be difficult to predict via neural networks, we first illustrate how to coarsely approximate these modes with a real-time numerical algorithm specifically designed to mimic the most important ballistic features of a classical numerical simulation. Although there is some flexibility in the choice of the numerical algorithm used as a proxy for full simulation, it is essential that the stability and accuracy be independent from any time step restriction or similar requirements in order to facilitate real-time performance. In order to reduce the number of degrees of freedom that require approximations to their dynamics, we simulate rigid frames and use skinning to reconstruct a rough approximation to a desirable mesh; as one might expect, neural-network-based skinning seems to perform better than linear blend skinning in this scenario. Improved high frequency deformations are subsequently added to the skinned mesh via a quasistatic neural network (QNN). In contrast to recurrent neural networks that require a plethora of training data in

order to adequately generalize to new examples, QNNs perform well with significantly less training data.

CCS Concepts: • **Computing methodologies** → **Animation; Neural networks; Physical simulation.**

Additional Key Words and Phrases: Cloth animation, deep learning, skinning

1 INTRODUCTION

Animation of digital clothing has been a captivating research area for decades due to its importance in creating realistic digital humans. While traditional physics-based simulation methods [Baraff and Witkin 1998; Bridson et al. 2002; Choi and Ko 2002] can generate high-fidelity results, the inability to achieve real-time performance at high resolutions restricts their utility in contemporary real-time applications such as video games, VR/AR, and virtual try-on systems. In light of recent advancements in GPU hardware, there has been a surge of interest in leveraging neural networks to approximate physics-based simulations, see e.g. [Lewin 2021; Patel et al. 2020; Pfaff et al. 2021; Raissi et al. 2019; Sanchez-Gonzalez et al. 2020; Santesteban et al. 2019]

Tight or close fitting garments such as shirts, pants, etc. typically exhibit only subtle dynamic behaviors; thus, capturing quasistatic shape information is more important than modelling the ballistic

Authors' addresses: Yongxu Jin, yxjin@stanford.edu, Stanford University, Stanford, California, USA and Epic Games, Cary, North Carolina, USA; Dalton Omens, domens@stanford.edu, Stanford University, Stanford, California, USA and Epic Games, Cary, North Carolina, USA; Zhenglin Geng, zhenglin.geng@epicgames.com, Epic Games, Cary, North Carolina, USA; Joseph Teran, jteran@math.ucdavis.edu, University of California, Davis, Davis, California, USA and Epic Games, Cary, North Carolina, USA; Abishek Kumar, Abishek.Kumar@sony.com, Sony Corporation of America, R&D US Laboratory, USA; Kenji Tashiro, Kenji.Tashiro@sony.com, Sony Corporation of America, R&D US Laboratory, USA; Ronald Fedkiw, rfedkiw@stanford.edu, Stanford University, Stanford, California, USA and Epic Games, Cary, North Carolina, USA.

motion, see e.g. [Bertiche et al. 2021a; Jin et al. 2020; Lahner et al. 2018; Patel et al. 2020]. Quasistatic shape information can be captured by various skinning techniques, by neural networks that lack temporal information (we will refer to these as quasistatic neural networks or QNNs), or by a combination of skinning and quasistatic neural network approaches. While some low-frequency vibration of tight-fitting clothing can be captured by underlying flesh motion (see e.g. [Jin et al. 2022]), modelling the pronounced ballistic motion associated with loose-fitting clothing such as skirts, dresses, capes, etc. is more challenging. Skinning and QNN based approaches have not been able to successfully model pronounced ballistic motion; thus, researchers have explored alternative network architectures that incorporate temporal history, most notably recurrent neural networks (RNNs), see e.g. [Pan et al. 2022; Santesteban et al. 2022; Zhang et al. 2021]. Unfortunately, the amount of training data required to robustly model temporal transitions between states (especially when considering the need for generalization) is significantly greater than that required to model the states themselves. Moreover, increased network capacity is required in order to properly capture the numerous state transitions present in this increased volume of training data. These issues typically cause recurrent neural network approaches to overfit and thus generalize poorly.

Since a physics-based simulation readily models ballistic motions but does not efficiently scale to a large number of degrees of freedom and neural networks readily deal with a large number of degrees of freedom but struggle with temporal state transitions, we pursue a more optimal hybrid approach that uses a small number of degrees of freedom physics simulation to capture dynamics and a neural network to capture a high resolution shape. In particular, we physically simulate such a low number of degrees of freedom that they are best viewed as virtual bones as opposed to being viewed as a subset of a higher resolution mesh (similar to [Pan et al. 2022; Zhao et al. 2023]); thus, we rely on skinning (driven by a neural network) in order to construct a coarse approximation to the desired mesh from the simulated degrees of freedom. Given this coarsely approximated dynamic mesh, a quasistatic neural network is then used to obtain a more desirable higher resolution mesh.

Since we rely on the neural network’s ability to capture the shape of the cloth, the physics simulation does not require all the usual (and computationally expensive) techniques for simulating stretching, bending, compression, etc.; thus, we devise a novel approach that connects our virtual bones (or rigid frames) into vertical rope chains. Each rope is designed to be inextensible yet shrinkable, avoiding undesirable locking or rubbery buckling artifacts (see [Jin et al. 2017] for detailed insights). Optional spring forces can be included in order to softly constrain the distances between different rope chains and/or to regulate the shrinking of each rope (if desired). Compared to low resolution cloth simulation, the rope chains can be robustly simulated with large time steps thus enabling real-time performance. Instead of simulating the rotational (in addition to translational) degrees of freedom typically required in order to skin a coarse mesh from virtual bones (or rigid frames), we utilize a neural network so that the garment can be skinned directly from the simulated translational degrees of freedom.

Collisions between the body and the rope chain degrees of freedom are facilitated via signed distance functions (SDFs), see e.g.

[Bridson et al. 2003]. In order to avoid computationally expensive grid-based SDFs, the SDF can be defined either by a set of closed-form primitives (desirable for real-time applications like video games) or by a neural network (see e.g. [Park et al. 2019; Remelli et al. 2020]). Similar collision treatment can also be applied to the degrees of freedom of the full cloth mesh. Both the skinning neural network and the QNN are trained with an additional PINN-style [Raissi et al. 2019] collision loss (using the SDF) in order to obtain network parameters that favor collision-free cloth mesh degrees of freedom; importantly, adding collisions in this fashion does not require modifications to the network architecture nor does it add any computational expense to inference.

To summarize our contributions:

- We propose a hybrid framework for animating loose-fitting clothing that blends together the efficacy of physics simulation for capturing ballistic motion and the efficiency of neural networks for skinning and shape inference.
- In particular, we propose a novel simulation method for low resolution (and loose-fitting) clothing via ballistic rope chains, which are used to reconstruct a full cloth mesh with the aid of neural networks for both skinning and shape inference.
- We propose a novel collision handling method with analytic SDFs, using history-based information in order to improve both robustness and efficiency for the sake of real-time applications.

2 RELATED WORK

Physics Simulation: The physical simulation of cloth has a long history in computer graphics, dating back to [Terzopoulos et al. 1987]; however, it gained significant popularity due to the implicit time integration approach proposed in [Baraff and Witkin 1998]. In order to overcome the overly-damped (underwater) appearance of implicit time integration, [Bridson et al. 2002, 2003] introduced a semi-implicit time integration approach (central differencing in computational mechanics) that is explicit on the elastic vibrational modes and implicit on the damping modes. Although offline methods could simulate very high resolution cloth even 15 years ago (see [Selle et al. 2008]), position based dynamics (starting with [Müller et al. 2007]) has been the method of choice for most real-time applications. Other interesting contributions include discussions on the buckling instability [Choi and Ko 2002], overcoming locking [Jin et al. 2017], etc.

Neural Physics: Many researchers have aimed to mimic physics simulations via neural networks and various other data-driven techniques. Early works include: [De Aguiar et al. 2010; Hahn et al. 2014] used a PCA subspace, [Guan et al. 2012] predicted a cloth mesh from pose history and body shape, [Kim et al. 2013] used motion graphs, and [Loper et al. 2015; Pons-Moll et al. 2015] used linear auto-regression. As deep learning gained popularity, a number of authors embraced neural networks. [Luo et al. 2018] used a neural network to add non-linear displacements on top of linear elasticity. [Holden et al. 2019] used a neural network in a PCA subspace to replace time integration. [Fulton et al. 2019; Tan et al. 2020; Wang et al. 2019] all aimed to integrate state transitions in a latent

space (see also [Zhang et al. 2021]). [Chentanez et al. 2020; Li et al. 2022; Pfaff et al. 2021; Sanchez-Gonzalez et al. 2020] all used graph neural networks, which can embrace the typical physics based simulation notion of a stencil (see also [Zheng et al. 2021]). [Grigorev et al. 2023; Santesteban et al. 2022] used a PINN-style objective function. Although PINNs (first proposed in [Raissi et al. 2019]) are self-supervised and as such do not require ground truth data, there is nothing special about their architecture implying that they need just as much training data as any other method in order to properly generalize to unseen data. [Shao et al. 2023] used Transformers. [Li et al. 2023] used three networks to capture static, coarse, and wrinkle dynamics separately. Most similar to our approach, [Diao et al. 2023; Pan et al. 2022; Zhao et al. 2023] used virtual bones, skinning, and/or super-resolution techniques; however, (unlike us) they used RNNs to animate the virtual bones.

Rigging and Skinning: There is a long history of rigging and skinning in computer graphics, although not necessarily geared towards cloth animation. We refer interested readers to [Magnenat et al. 1988] for linear blend skinning, [Lewis et al. 2000] for pose space deformation, [Kurihara and Miyata 2004] for weighted pose space deformation, [Kavan et al. 2007, 2008] for dual quaternion skinning, and [Rumman and Fratarcangeli 2017] for a survey. Other interesting works include the parametric body models in [Angelov et al. 2005] (SCAPE) and [Loper et al. 2015] (SMPL) and the joint extraction in [Le and Deng 2012] (SSDR). It is difficult to skin clothing (especially when it is loose-fitting) using standard (non-neural) skinning techniques; however, see e.g. [Wang et al. 2010; Xu et al. 2014].

Neural Shape: There have been a number of efforts to infer shape (and appearance, see [Lahner et al. 2018]) using neural networks. [Bailey et al. 2018] added per-vertex displacements on top of the skinned body mesh, and [Bailey et al. 2020] similarly added per-vertex displacements on top of a skinned face mesh. [Jin et al. 2022] also added per-vertex displacements on top of skinned body mesh, but augmented these with dynamic motion from analytic springs. For cloth, there have been various attempts to create a high resolution mesh from the physics simulation of a coarser mesh, see e.g. [Chentanez et al. 2020; Kavan et al. 2011; Oh et al. 2018]. Inferring cloth from body pose and shape alone (without a coarse simulation mesh) is significantly more difficult, see e.g. [Bertiche et al. 2021a; Gundogdu et al. 2019; Jin et al. 2020; Lee et al. 2023; Lewin 2021; Li et al. 2024; Patel et al. 2020; Santesteban et al. 2019; Tan et al. 2022].

Collisions: The successful approach to cloth-cloth self collisions using continuous collision detection (CCD) in [Bridson et al. 2002] (which leveraged [Provot 1997]) led to a plethora of work on improving the efficiency of $O(n \log n)$ collision detection (see e.g. [Govindaraju et al. 2005; Li et al. 2020; Sud et al. 2006; Tang et al. 2014, 2018]); however, for cloth-body collisions, signed distance functions (SDFs) remain prevalent due to their more efficient $O(1)$ cost (see e.g. [Bridson et al. 2003]). The main drawback of SDFs is that the three dimensional discretization of the volumetric field is expensive to load and store in memory; thus, analytic SDFs are more popular for real-time applications (see e.g. [Blinn 1982; Nishimura et al. 1985;



Fig. 2. The loose-fitting garments that we use for numerical experiments. The cape mesh consists of 12690 vertices, and we define 10 rope chains with 13-15 virtual bones in each chain (reducing the total DOFs by a factor of approximately 90). The skirt mesh consists of 18546 vertices, and we define 26 rope chains with 9 virtual bones in each chain (reducing the total DOFs by a factor of approximately 80). Importantly, the large reduction in the number of DOFs is highly beneficial for both RAM and cache performance, not just CPU performance. Note that the unattached virtual bones near the top of both the cape and the skirt are not simulated, but they will be used for skinning (see Section 7).

Wyvill et al. 1986]). Neural network approximations to SDFs have the potential to be efficient enough to be used in real-time applications. Inference is typically fast enough, but the amount of network parameters required (or new network parameters required, when switching from one SDF to another) needs to be small enough to be efficiently loaded and/or stored in memory. We refer the interested reader to [Mehta et al. 2022; Park et al. 2019; Remelli et al. 2020; Saito et al. 2019; Shen et al. 2021; Wu et al. 2023] for various details (and discussions on differentiability).

Physics-Informed Neural Networks (PINNs): For neural network inferred cloth, the computational burden from processing collision-free training data. Unfortunately, regularization (which is generally necessary and desirable) prevents inferred cloth from being interpenetration-free even when the training data is interpenetration-free. Thus, PINN-style [Raissi et al. 2019] collision losses can be quite useful during training (see [Bertiche et al. 2021a,b; Gundogdu et al. 2019; Santesteban et al. 2022, 2021]), as they allow one to increase the penalty on cloth-body interpenetrations without forcing overfitting to the interpenetration-free training data. The PINN losses can be made as stiff as desired while otherwise maintaining desirable regularization on the deviation of the cloth from the training data positions.

3 ROPE CHAIN SIMULATION

Given a garment mesh, we define a set of virtual bones distributed across the garment (either manually or by a procedural algorithm such as SSDR [Le and Deng 2012]); then, the virtual bones are interconnected vertically to form a set of simulatable rope chains (see Figure 2). Not only does this significantly reduce the number of degrees of freedom that need to be simulated, but (we argue that) the rope chains provide a much better approximation to the desired ballistic degrees of freedom than a rubbery mass-spring mesh does: Rope chains can be made to swing and rotate freely,

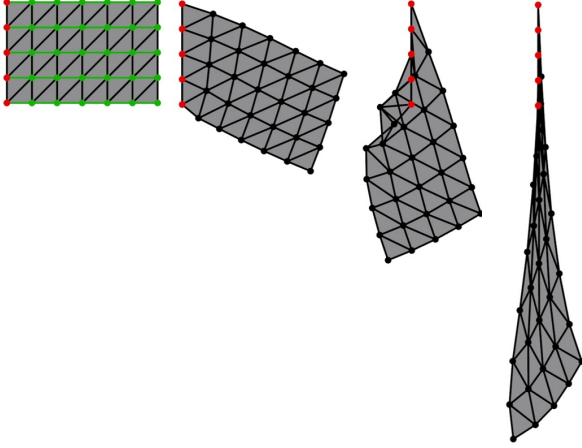


Fig. 3. The far left subfigure shows a a coarsely discretized mesh with position constraints on the five red nodes. The next three subfigures show the results of steady state simulations using a decreasing spring stiffness (from left to right). The final subfigure shows a rope chain simulation (the rope chains are shaded green) of the same degrees of freedom. The mass-spring simulations lock with stiffer springs and overstretch with weaker springs. The spring stiffness in the middle subfigure was chosen to approximately match the downward stretching extent of the rope chain simulation, which is what one would expect without overstretching; however, locking occurs since the springs are still too stiff.

whereas a mass-spring system follows linearized rotations resisted by spring stretching. Rope chains can be made to buckle freely, whereas a mass-spring system over-resists buckling (locking when under-discretized, see e.g. [Jin et al. 2017]). Enforcing inextensibility is trivial (from root to tip) for a rope chain, whereas various ad-hoc techniques are required in order to prevent over-stretching for a mass-spring simulation. Etc. See Figure 3.

A semi-implicit Newmark style time integration scheme is used separately for each rope chain (see e.g. [Bridson et al. 2003]):

- (1) $\vec{v}^{n+\frac{1}{2}} = \vec{v}^n + \frac{\Delta t}{2} \frac{\vec{F}(\vec{x}^n, \vec{v}^n)}{M}$
- (2) $\vec{x}^{n+1} = \vec{x}^n + \Delta t \vec{v}^{n+\frac{1}{2}}$
- (3) Resolve collisions, perturbing \vec{x}^{n+1} and $\vec{v}^{n+\frac{1}{2}}$
- (4) $\vec{v}^{n+1} = \vec{v}^{n+\frac{1}{2}} + \frac{\Delta t}{2} \frac{\vec{F}(\vec{x}^{n+1}, \vec{v}^{n+\frac{1}{2}})}{M}$

This is often referred to as central differencing in the computational mechanics literature. Central differencing preserves rich high-frequency dynamic motion significantly better than fully-implicit methods (such as backward Euler) do. The velocity updates (steps 1 and 4) are discussed in detail in Section 4, the position update (step 2) is discussed in detail in Section 5, and collisions (step 3) are discussed in detail in Section 6. See Figure 4.

4 VELOCITY UPDATE

Given a rope chain, let $\vec{x}_0, \dots, \vec{x}_m$ denote the virtual bones from root to tip where \vec{x}_0 is kinematically constrained to follow some part of the body (or some other object). The magnitude of each $\vec{l}_i = \vec{x}_i - \vec{x}_{i-1}$ should never exceed the maximal length $l_{max,i}$ of the corresponding

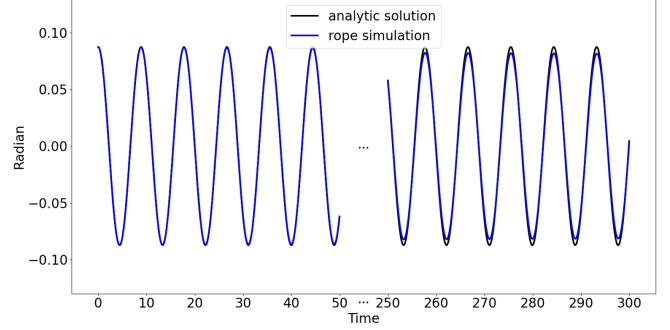


Fig. 4. In this figure, we simulate two virtual bones connected by a single rope with the top virtual bone fixed and the bottom virtual bone free to rock back and forth as a pendulum. The results compare well to the analytic solution for pendulum motion for both shorter times (left) and longer times (right), illustrating the efficacy of our numerical approach.

rope; however, there is no penalty for slack ($|\vec{l}_i| = l_i < l_{max,i}$) in the rope. Except for \vec{x}_0 , various external forces $\vec{F}_{ext,i}$ are applied to the virtual bones. Examples include gravity $\vec{F}_g = M_i \vec{g}$, wind drag $\vec{F}_{wind} = -c_{wind}(\vec{v}_i - \vec{v}_{wind})$, etc. In order to prevent a rope chain from deviating too far from its neighboring rope chains, springs can be attached laterally connecting each virtual bone to its neighbors on neighboring rope chains. We treat these as soft constraints, meant to influence but not overly dictate the simulation; thus, they are added to $\vec{F}_{ext,i}$ and given the same relative importance as gravity, wind drag, and other similar forces. One may also desire forces that aim to preserve rest angles between consecutive pairs of virtual bones, in order to coerce the cloth towards its rest shape. These forces would also be included in $\vec{F}_{ext,i}$.

When a rope reaches its maximal length $l_{max,i}$, the two virtual bones it attaches to will rotate around each other. The magnitude of the centripetal force required to maintain this rotation is

$$F_{c,i} = M_{i-1} \frac{|\vec{v}_{i-1} - \vec{v}_c - \left((\vec{v}_{i-1} - \vec{v}_c) \cdot \hat{l}_i \right) \hat{l}_i|^2}{|\vec{x}_{i-1} - \vec{x}_c|} = M_i \frac{|\vec{v}_i - \vec{v}_c - \left((\vec{v}_i - \vec{v}_c) \cdot \hat{l}_i \right) \hat{l}_i|^2}{|\vec{x}_i - \vec{x}_c|} \quad (1)$$

where $\vec{x}_c = \frac{M_{i-1}\vec{x}_{i-1} + M_i\vec{x}_i}{M_{i-1} + M_i}$ is the center of mass, $\vec{v}_c = \frac{M_{i-1}\vec{v}_{i-1} + M_i\vec{v}_i}{M_{i-1} + M_i}$ is the velocity at the center of mass, and $\hat{l}_i = \frac{\vec{l}_i}{l_i}$ is unit length (i.e. a direction). For the first rope, which connects the kinematic \vec{x}_0 with \vec{x}_1 , $\vec{x}_c = \vec{x}_0$ and $\vec{v}_c = \vec{v}_0$ due to $M_0 = \infty$ (note that second line of Equation 1 needs to be used to calculate $F_{c,1}$, in order to avoid dealing with L'Hopital's rule in the first line).

When a rope reaches its maximal length $l_{max,i}$, an additional tension force with magnitude $T_i \geq 0$ is added to the non-kinematic virtual bones it attaches to (the kinematic root ignores these forces). The net force in the virtual bones can be defined via

$$\vec{F}_{net,i} = \vec{F}_{ext,i} - T_i \hat{l}_i + T_{i+1} \hat{l}_{i+1} \quad (2a)$$

$$\vec{F}_{net,m} = \vec{F}_{ext,m} - T_m \hat{l}_m \quad (2b)$$

where $i \in \{1, \dots, m-1\}$ and $T_i = 0$ whenever $l_i < l_{max,i}$. In order to preserve the rotational motion for each taut rope,

$$\vec{F}_{net,1} \cdot \hat{l}_1 \leq -F_{c,1} + M_1 \ddot{x}_0 \cdot \hat{l}_1 \quad (3a)$$

$$\vec{F}_{net,i} \cdot \hat{l}_i - \vec{F}_{net,i-1} \cdot \hat{l}_i \leq -2F_{c,i} \quad (3b)$$

where $i \in \{2, \dots, m\}$ and the \ddot{x}_0 term accounts for the motion of the kinematic root. Substituting Equations 2a and 2b into Equations 3a and 3b gives

$$-T_1 + \hat{l}_2 \cdot \hat{l}_1 T_2 \leq -\vec{F}_{ext,1} \cdot \hat{l}_1 - F_{c,1} + M_1 \ddot{x}_0 \cdot \hat{l}_1 \quad (4a)$$

$$\hat{l}_{i-1} \cdot \hat{l}_i T_{i-1} - 2T_i + \hat{l}_{i+1} \cdot \hat{l}_i T_{i+1} \leq (\vec{F}_{ext,i-1} - \vec{F}_{ext,i}) \cdot \hat{l}_i - 2F_{c,i} \quad (4b)$$

$$\hat{l}_{m-1} \cdot \hat{l}_m T_{m-1} - 2T_m \leq (\vec{F}_{ext,m-1} - \vec{F}_{ext,m}) \cdot \hat{l}_m - 2F_{c,m} \quad (4c)$$

where $i \in \{2, \dots, m-1\}$. This tri-diagonal linear system of inequalities (for the unknown tension) decouples into separate blocks whenever a slack rope has $l_i < l_{max,i}$ or two consecutive ropes are orthogonal (with a dot product of zero). For computational efficiency, we iterate these equations in tip-to-root order (from bottom to top in Equation 4) using Gauss-Seidel; for most real-time applications, typically only one tip-to-root sweep is required. In particular, we rewrite Equations 4a, 4b, and 4c in reverse order as

$$T_m \geq \frac{(\vec{F}_{ext,m} - \vec{F}_{ext,m-1}) \cdot \hat{l}_m + 2F_{c,m} + \hat{l}_{m-1} \cdot \hat{l}_m T_{m-1}}{2} \quad (5a)$$

$$T_i \geq \frac{(\vec{F}_{ext,i} - \vec{F}_{ext,i-1}) \cdot \hat{l}_i + 2F_{c,i} + \hat{l}_{i-1} \cdot \hat{l}_i T_{i-1} + \hat{l}_{i+1} \cdot \hat{l}_i T_{i+1}}{2} \quad (5b)$$

$$T_1 \geq \vec{F}_{ext,1} \cdot \hat{l}_1 + F_{c,1} - M_1 \ddot{x}_0 \cdot \hat{l}_1 + \hat{l}_2 \cdot \hat{l}_1 T_2 \quad (5c)$$

and enforce them sequentially (from top to bottom in Equation 5) by choosing each T_i equal to the larger between zero and right hand side.

After solving for T_i via Equation 5, Equation 2 can be used to find the net force $\vec{F}_{net,i}$ on each non-kinematic virtual bone. Given $\vec{F}_{net,i}$ for each non-kinematic virtual bone, the velocity can be updated in any order (for both step 1 and step 4 of the time integration); in addition, the velocity of the kinematic virtual bone (the root) should be updated as well.

The updated velocities may be subject to an additional instantaneous impulse of magnitude $I_i \geq 0$ whenever a rope is at its maximal length $l_{max,i}$. Let $\vec{v}_{pre,i}$ and $\vec{v}_{post,i}$ be the velocity before and after (respectively) this instantaneous exchange of momentum; then, the impulses along the ropes are applied via

$$M_i \vec{v}_{post,i} = M_i \vec{v}_{pre,i} - I_i \hat{l}_i + I_{i+1} \hat{l}_{i+1} \quad (6a)$$

$$M_m \vec{v}_{post,m} = M_m \vec{v}_{pre,m} - I_m \hat{l}_m \quad (6b)$$

where $i \in \{1, \dots, m-1\}$ and $I_i = 0$ whenever $l_i < l_{max,i}$. Note that $\vec{v}_{post,0} = \vec{v}_{pre,0}$, since $M_0 = \infty$. In order to prevent each taut rope from overstretching,

$$(\vec{v}_{post,i} - \vec{v}_{post,i-1}) \cdot \hat{l}_i \leq 0 \quad (7)$$

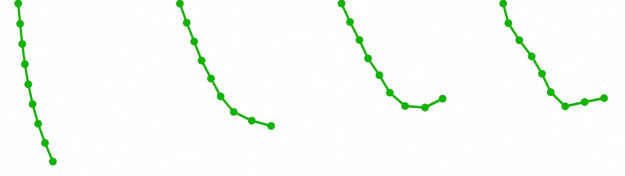


Fig. 5. Motion of a single swinging rope chain, showcasing varying numbers of Gauss-Seidel iterations. Left to right: 1, 5, 10 iterations, and iterating until the relative error is smaller than a tolerance of 10^{-6} . With more iterations, the rope chain is less damped (as expected). The same number of iterations (or the same tolerance) was used for both the tension and impulse computations. Note that it might be more efficient (depending on the application) to use a different number of iterations on the tension and impulse computations.

must hold, where $i \in \{1, \dots, m\}$. Substituting Equations 6a and 6b into Equation 7 gives

$$-\frac{1}{M_1} I_1 + \frac{\hat{l}_2 \cdot \hat{l}_1}{M_1} I_2 \leq (\vec{v}_{pre,0} - \vec{v}_{pre,1}) \cdot \hat{l}_1 \quad (8a)$$

$$\frac{\hat{l}_{i-1} \cdot \hat{l}_i}{M_{i-1}} I_{i-1} - \left(\frac{1}{M_{i-1}} + \frac{1}{M_i}\right) I_i + \frac{\hat{l}_{i+1} \cdot \hat{l}_i}{M_i} I_{i+1} \leq (\vec{v}_{pre,i-1} - \vec{v}_{pre,i}) \cdot \hat{l}_i \quad (8b)$$

$$\frac{\hat{l}_{m-1} \cdot \hat{l}_m}{M_{m-1}} I_{m-1} - \left(\frac{1}{M_{m-1}} + \frac{1}{M_m}\right) I_m \leq (\vec{v}_{pre,m-1} - \vec{v}_{pre,m}) \cdot \hat{l}_m \quad (8c)$$

where $i \in \{2, \dots, m-1\}$. This tri-diagonal linear system of inequalities decouples into separate blocks whenever a slack rope has $l_i < l_{max,i}$ or two consecutive ropes are orthogonal. For computational efficiency, we iterate these equations in root-to-tip order (from top to bottom in Equation 8) using Gauss-Seidel; for most real-time applications, typically only one root-to-tip sweep is required. In particular, we rewrite 8a, 8b, and 8c as

$$I_1 \geq M_1 \left((\vec{v}_{pre,1} - \vec{v}_{pre,0}) \cdot \hat{l}_1 + \frac{\hat{l}_2 \cdot \hat{l}_1}{M_1} I_2 \right) \quad (9a)$$

$$I_i \geq \frac{M_{i-1} M_i}{M_{i-1} + M_i} \left((\vec{v}_{pre,i} - \vec{v}_{pre,i-1}) \cdot \hat{l}_i + \frac{\hat{l}_{i-1} \cdot \hat{l}_i}{M_{i-1}} I_{i-1} + \frac{\hat{l}_{i+1} \cdot \hat{l}_i}{M_i} I_{i+1} \right) \quad (9b)$$

$$I_m \geq \frac{M_{m-1} M_m}{M_{m-1} + M_m} \left((\vec{v}_{pre,m} - \vec{v}_{pre,m-1}) \cdot \hat{l}_m + \frac{\hat{l}_{m-1} \cdot \hat{l}_m}{M_{m-1}} I_{m-1} \right) \quad (9c)$$

and enforce them sequentially (from top to bottom in Equation 9) by choosing each I_i equal to the larger between zero and right hand side.

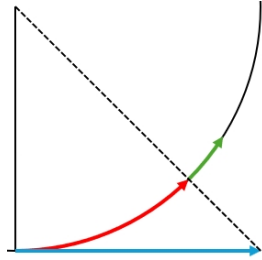
Note that we chose tip to root for the tension so that each virtual bone feels the weight of all the virtual bones below it even when executing only one iteration. Conversely, we chose root to tip for the impulse since it has been argued (and shown) to work well for contact resolution in prior works (see e.g. [Guendelman et al.

2003]). Figure 5 illustrates the results one might typically expect with different numbers of iterations.

5 POSITION UPDATE

In contrast to the tension and impulse computations discussed in Section 4 which address force and velocity constraints respectively, a stricter approach is desirable for position constraints (especially to avoid errors in the rendered visualizations); thus, we execute one sweep from root to tip on the length of each rope in order to prevent it from exceeding its maximum length. Each virtual bone is updated from its time t^n position to its time t^{n+1} position by considering both its time $t^{n+\frac{1}{2}}$ velocity (computed as described in Section 4) and the rope constraint on its position relative to the previously updated virtual bone (in the root to tip sweep). That is, \vec{x}_i^n is updated to \vec{x}_i^{n+1} by considering both $\vec{v}_i^{n+\frac{1}{2}}$ and the rope that connects the virtual bone to \vec{x}_{i-1}^{n+1} .

When the rope is slack, the virtual bone’s position can evolve freely with no hindrance from the constraint; however, when the rope is taut, the virtual bone is constrained to rotate on the sphere about \vec{x}_{i-1}^{n+1} . Approximating this with an evolve-and-project strategy damps the rotation to the linearized rotation. This can be seen by projecting the distance moved in a linearized rotation (colored blue in the figure) back onto a great circle and noting that the arc length thus traversed (colored red in the figure) is smaller than the distance covered in the linearized rotation, which is the arc length distance that should have been traversed (the sum of red and green colored arcs in the figure). Thus, we address the constrained motion with a non-linearized (actual) rotation.



The tautness of the rope is governed by the quadratic function

$$f(s) = |\vec{x}_i^n + s\vec{v}_i^{n+\frac{1}{2}} - \vec{x}_{i-1}^{n+1}|^2 - l_{max,i}^2 \quad (10)$$

where $f(s) < 0$ indicates slack and $f(s) > 0$ indicates overstretching. When $f(\Delta t) \leq 0$, the rope is not overstretching at the end of the time step and $\vec{x}_i^{n+1} = \vec{x}_i^n + \Delta t\vec{v}_i^{n+\frac{1}{2}}$ is accepted as the final position. Otherwise, when $f(\Delta t) > 0$, we compute the largest root s_{root} in the interval $[0, \Delta t]$. If there is no root in the interval, then we set $s_{root} = 0$ and project the overstretching \vec{x}_i^n back onto the surface of the sphere via

$$\vec{x}_i^n \leftarrow \vec{x}_{i-1}^{n+1} + \frac{\vec{x}_i^n - \vec{x}_{i-1}^{n+1}}{|\vec{x}_i^n - \vec{x}_{i-1}^{n+1}|} l_{max,i} \quad (11)$$

so that it is no longer overstretching. In the interval $[0, s_{root}]$, the virtual bone is allowed to move unhindered by the constraint via $\vec{x}_i^{s_{root}} = \vec{x}_i^n + s_{root}\vec{v}_i^{n+\frac{1}{2}}$. Note that this intentionally ignores any overstretching in $[0, s_{root}]$, since such overstretching is overcome automatically and may only be the (spurious) result of updating the virtual bones one at a time (from root to tip) as opposed to uniformly.

In the interval $[s_{root}, \Delta t]$, the virtual bone is constrained to rotate on the sphere centered at \vec{x}_{i-1}^{n+1} of radius $l_{max,i}$. Given $\vec{l}_i^{s_{root}} =$

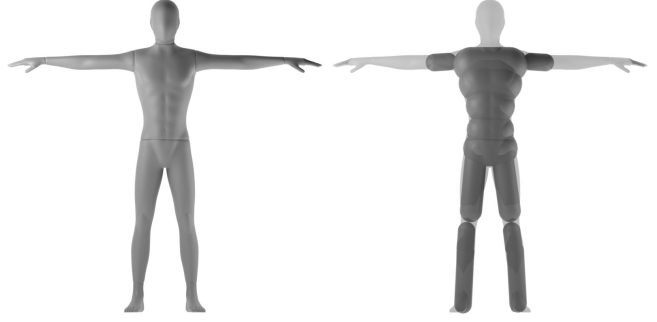


Fig. 6. For the sake of computational efficiency, we represent the volumetric body (left) with a number of analytically defined SDFs (right). Although other representations (three dimensional grid discretizations, neural representations, etc.) are compatible with our approach, they incur higher computational costs.

$\vec{x}_i^{s_{root}} - \vec{x}_{i-1}^{n+1}$ and $\hat{l}_i^{s_{root}} = \frac{\vec{l}_i^{s_{root}}}{|\vec{l}_i^{s_{root}}|}$, the tangential velocity

$$\vec{v}_T = \vec{v}_i^{n+\frac{1}{2}} - (\vec{v}_i^{n+\frac{1}{2}} \cdot \hat{l}_i^{s_{root}}) \hat{l}_i^{s_{root}} \quad (12)$$

is used to determine the distance $d_T = |\vec{v}_T|(\Delta t - s_{root})$ the virtual bone rotates on the great circle specified by the direction $\hat{v}_T = \frac{\vec{v}_T}{|\vec{v}_T|}$. A rotation matrix R is defined to rotate the virtual bone by an amount $\theta = \frac{d_T}{l_{max,i}}$ about the axis $\hat{l}_\theta = \hat{l}_i^{s_{root}} \times \hat{v}_T$ via

$$\vec{l}_i^{n+1} = R(\theta, \hat{l}_\theta) \vec{l}_i^{s_{root}} \quad (13)$$

to obtain $\vec{x}_i^{n+1} = \vec{x}_{i-1}^{n+1} + \vec{l}_i^{n+1}$.

After the position update, the velocities may no longer satisfy the constraint preventing overstretching (see Equation 7). Thus, new impulses can be computed and applied (following the discussion in the second half of Section 4). Alternatively, impulses can instead be computed and applied after resolving collisions, both after the position update and after resolving collisions, or deferred entirely (and left unmodified until the end of second velocity update).

6 COLLISIONS

Generally speaking, we follow the method in [Bridson et al. 2003] detecting and processing collisions between each non-kinematic virtual bone and each signed distance function (SDF). Although this approach has quite efficient $O(1)$ processing time for each virtual bone, it is computationally expensive to load three dimensional SDF discretizations into memory; in addition, the limited memory availability in most real-time systems makes it infeasible to store the SDFs persistently. Thus, we avoid these costly three dimensional discretizations by utilizing SDFs that can be defined analytically (see e.g. [Blinn 1982; Nishimura et al. 1985; Wyvill et al. 1986]). See Figure 6. Alternatively, a number of authors have aimed to represent SDFs via neural networks (see e.g. [Park et al. 2019; Remelli et al. 2020]). If the number of parameters in the neural network can be made to be much smaller than an equivalently accurate three dimensional discretization, then the computational costs associated with high demands on memory could be avoided. Instead of aiming to make each neural SDF utilize less memory than its equivalently accurate

three dimensional discretization, one could aim to minimize the additional memory burden incurred by switching from one neural SDF to another (e.g. by using shape descriptors).

Motivated by the cloth-object collision discussion in [Selle et al. 2008], we propose a modification to [Bridson et al. 2003] in order to obtain more robust behavior for real-time applications with coarse discretizations and large time steps. In the standard approach, an initially non-interpenetrating particle that ends up in the interior of an SDF is pushed outwards in the $\nabla\phi$ direction until it reaches the surface of the SDF (or a bit further than the surface when aiming for wrinkle preservation as discussed in [Bridson et al. 2003]). In contrast, a real-world particle is unable to penetrate into the interior of an object and instead collides with the surface and responds accordingly. In the limit as the time step goes to zero and the number of points used to represent the surface goes to infinity, the standard numerical approach converges to the correct real-world solution (roughly speaking, ignoring the inability to properly model friction, microscopic structure, etc.). However, the numerical errors are exacerbated by the large time steps and the coarse surface discretizations utilized for real-time applications. Although continuous collision detection (CCD) could be used to increase the accuracy while maintaining a large time step, CCD is too computationally burdensome for most real-time applications (although progress is being made, see e.g. [Li et al. 2020] and the references therein).

The standard approach of evolving a particle into an interpenetrating state and subsequently pushing it outwards in the $\nabla\phi$ direction can be thought of as a predictor-corrector method modeling the actual path of the particle (the path that CCD would aim to trace out). Aiming to preserve the computational efficiency of the predictor, we propose modifying the corrector in order to obtain a more accurate final state. This can be done efficiently by choosing a more appropriate direction for push out than $\nabla\phi$. In fact, $\nabla\phi$ can be highly erroneous when objects are thin (causing a particle to be pushed to the wrong side) or have high curvature (causing a particle to be pushed to the wrong direction); moreover, these errors are exacerbated by the larger time steps typically used in real-time applications. Given limited information, our ansatz is that the safest push out direction is the reverse direction along the path the particle traversed as it penetrated into the collision body. At the very least, this aims to return the particle to the point where a CCD collision would have occurred.

Assuming the collision body is stationary, the reverse path out of the collision body back towards the CCD collision point has direction $\vec{r} = \vec{x}^n - \vec{x}^{n+1}$ where \vec{x}^{n+1} is the predicted position of the particle (penetrating into the collision body). The main difficulty associated with using this direction is that it is unclear how far the particle should move. There are several options for addressing this. One could use the local value of $|\phi|$ as usual, but this does not necessarily alleviate interpenetration when $\hat{r} = \frac{\vec{r}}{|\vec{r}|}$ and $\nabla\phi$ point in different directions. Notably, the local value of $|\phi|$ is always too small, except when $\hat{r} = \nabla\phi$ in which case the particle should exactly reach the surface of the collision body. Therefore, one could iterate the push out a few times in order to better approach the surface. In addition, one could use a small $\epsilon > 0$ to augment the local value of $|\phi|$. This is roughly equivalent to using an SDF thickened by ϵ or

to pushing the particle outwards to the $\phi = \epsilon$ isocontour. Finally, note that one could use line search (perhaps via bisection), which is equivalent to CCD for the simple case when the collision body is stationary (CCD is typically much cheaper in this simple case).

When the collision body is moving, \vec{x}^n is not necessarily non-interpenetrating (since the collision body may move to cover it); in such a scenario, \hat{r} is no longer guaranteed to be a suitable replacement for $\nabla\phi$. Fortunately, this is easily remedied by analyzing the problem in the moving frame of the collision body. As the collision body moves and deforms from time t^n to t^{n+1} , we embed the particle to move with it. This guarantees that the new particle location, denoted \vec{x}_B^n , is non-interpenetrating. For example, when the collision body moves rigidly, that same rigid motion is applied to \vec{x}^n to obtain \vec{x}_B^n . For deforming and/or skinned collision bodies, the deformation/skinning needs to be extended to \vec{x}^n in order to obtain \vec{x}_B^n . This allows $\vec{r} = \vec{x}_B^n - \vec{x}^{n+1}$ to be used as a valid push out direction.

After the position \vec{x}^{n+1} is modified to be collision-free, the velocity $\vec{v}^{n+\frac{1}{2}}$ is modified to ensure that the relative normal velocity $(\vec{v}^{n+\frac{1}{2}} - \vec{v}_\phi) \cdot \hat{N}$ does not point into the SDF via

$$v_N^{new} = \max(\vec{v}^{n+\frac{1}{2}} \cdot \hat{N}, \vec{v}_\phi \cdot \hat{N}) \quad (14)$$

where \vec{v}_ϕ is the velocity of the (extended, if necessary) collision body at \vec{x}^{n+1} , and \hat{N} may be chosen as either $\nabla\phi$ or \hat{r} . The relative tangential velocity

$$\vec{v}_{rel,T} = \vec{v}^{n+\frac{1}{2}} - \vec{v}^{n+\frac{1}{2}} \cdot \hat{N} - \vec{v}_{\phi,T} \quad (15)$$

is defined using the tangential velocity $\vec{v}_{\phi,T} = \vec{v}_\phi - \vec{v}_\phi \cdot \hat{N}$ of the (extended, if necessary) collision body at \vec{x}^{n+1} . When the friction coefficient μ is non-zero, the relative tangential velocity is modified via

$$\vec{v}_T^{new} = \vec{v}_{\phi,T} + \max(0, 1 - \mu \frac{v_N^{new} - \vec{v}^{n+\frac{1}{2}} \cdot \hat{N}}{|\vec{v}_{rel,T}|}) \vec{v}_{rel,T} \quad (16)$$

as suggested by [Bridson et al. 2002]. The final post collision velocity is given by $v_N^{new} \hat{N} + \vec{v}_T^{new}$. See Figure 7.

The collisions are processed sequentially from root to tip. Since collisions alter the positions of the virtual bones, length constraints are enforced in this step as well. This is accomplished by adjusting the position of a virtual bone via $\vec{x}_i^{new} = \vec{x}_{i-1} + l_{max,i} \hat{l}_i$ whenever $l_i > l_{max,i}$. Of course, this can create new collisions, so back-and-forth iteration is desirable. The root to tip sweep is done only once, and any back-and-forth iteration between the collision and the length constraint happens only once for each virtual bone. We recommend starting this iteration with the length constraint, since it may remove the need for collisions. We also stress the importance of finishing this iteration with the collision check in order to preserve a non-interpenetrating state.

7 NEURAL SKINNING

After each frame of rope chain simulation, a full cloth mesh needs to be reconstructed for rendering. After extensive experimentation, we were not able to obtain reasonable results via any of the standard skinning methods (such as LBS [Magnenat et al. 1988] or Dual Quaternion Skinning [Kavan et al. 2007]). We were also unable to

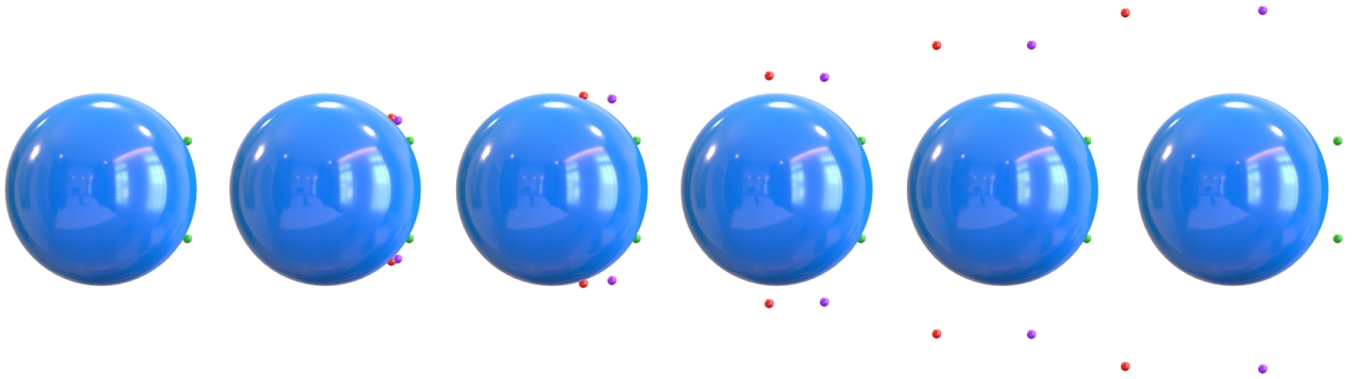


Fig. 7. Time evolution of a sphere colliding with six particles (6 frames are depicted). The red particles use the $\nabla\phi$ direction for both push out and velocity projection (as is typical), the purple particles use \hat{r} for push out and $\nabla\phi$ for velocity projection, and the green particles use \hat{r} for both push out and velocity projection. Note how replacing $\nabla\phi$ with \hat{r} prevents the particles from quickly working their way around the sphere. In fact, the green particles maintain a persistent contact with the sphere until it stops moving shortly before the last frame (even though friction is not used in this example). The behavior of the green particles is highly preferable to that of the red (and purple) particles when considering collisions between clothing and the human body.

remedy these issues with a corrective quasistatic neural network (see Section 8). The difficulties are likely due to the rope chain simulation’s inability to produce good rotational information for the virtual bones, even with various procedural modifications. Thus, we took an alternative approach that utilizes a neural network to infer PCA coefficients for the cloth mesh from the virtual bone translational degrees of freedom (only). This resulted in a mesh suitable enough for a corrective QNN to operate on (see Section 8).

For each cloth mesh under consideration, we utilize on the order of 5000 frames of simulated data (any offline simulation system will do) in order to construct a standard PCA model based on non-rigid displacements from the cloth rest state. The rest state of the cloth mesh is defined by its steady-state draped position in the rest pose of the body. Given an animated body pose, the rigid component of the cloth displacement is calculated as the rigid displacement of a key body part (the neck for the cape and the pelvis for the skirt) and removed from the cloth displacement in order to obtain its non-rigid displacement. About 100 PCA basis functions are retained for neural skinning. When the cloth meshes were converted to rope chains (see Figure 2), not all virtual bones were simulated (see the non-interconnected virtual bones in Figure 2); however, these virtual bones are needed in order to reconstruct the full cloth mesh and as such are also used as input into the neural skinning network. Given non-rigid displacements of the virtual bones from their positions in the cloth mesh rest state (their rigid component is identical to that used for the cloth mesh), the neural skinning network is trained to infer the approximately 100 PCA coefficients used to reconstruct the full cloth mesh.

We utilize a lightweight 2-layer MLP with 500 neurons per layer. In order to train the network, the same 5000 frames of simulation data (previously described) is used for supervision. The virtual bones are embedded in the cloth rest state and barycentrically enslaved to move with the simulation data yielding the inputs for the network. For each frame utilized in the data term of the loss function, the network-inferred PCA coefficients are used to reconstruct a cloth

mesh that is compared to the simulation ground truth vertex-by-vertex via a standard L2 norm. Importantly, each frame is treated as non-sequential in order to reduce the need for a higher capacity neural network, minimize the burden associated with collecting more training data, and avoid unnecessary overfitting. We did not find the need to add any additional terms (such as Laplacians) that would regularize the cloth mesh, since the use of a PCA model already provides sufficient regularization.

Even when the ground truth cloth meshes used in training do not interpenetrate the body, the inferred results will typically contain interpenetrations. This is caused by the regularization used to combat overfitting and to increase the efficacy of generalization to unseen data. In order to alleviate interpenetration without adversely affecting desirable regularization, we include a PINN-style collision loss during training. When a cloth vertex is found to be interpenetrating, we calculate a suitable non-interpenetrating position for that vertex (using push out) and include the difference between the vertex and its non-interpenetrating state in the PINN-style collision loss. The non-interpenetrating state can be calculated using $\nabla\phi$ as the push out direction along with the ϕ value (with or without iteration) or CCD to calculate the push out distance. Given the potentially large inaccuracy of the cloth state during training, $\nabla\phi$ often points in an unhelpful direction; thus, we instead chose an alternative push out direction \hat{r} pointing from the current position to the ground truth position. Note that it can be desirable for the non-interpenetrating state to be well-separated from the collision body (not just on the zero-isocontour) in order to create a buffer on the vertices that helps to alleviate edge interpenetrations (and/or to preserve wrinkling, see e.g. [Bridson et al. 2003]). Since we detach the non-interpenetrating state from the automatic differentiation graph, an interpenetrating vertex’s contribution to the gradient from the PINN-style collision loss is parallel to its contribution from the data term. This can be interpreted as increasing the importance of matching the ground truth for vertices that are interpenetrating as compared to vertices that are non-interpenetrating; in fact, we use a weight of 1000 on



Fig. 8. Top row: first five principle components of the neural skinning PCA model for the cape. Bottom row: first five principle components of the neural shape PCA model for the cape. All of the images depict the augmentation of the rest shape cloth mesh by the PCA displacements, even though the displacements are added to the skinned mesh (not the rest state mesh) during neural shape inference. The PCA model used for skinning tends to capture low-frequency deformations, while the PCA model used for shape inference is better suited for capturing higher-frequency deformations.

the PINN-style collision loss and a weight of only 0.1 for the data term.

It is important to note that there is a large discrepancy between the virtual bone configurations that arise from rope chain simulations and the configurations in the training data, which are obtained by barycentrically embedding virtual bones in a mass-spring cloth simulation mesh. That is, we are aiming to make the network generalize well to (sometimes significantly) out-of-distribution data. The usual process of utilizing holdout data does help to increase the ability of a network to generalize to unseen data; however, the errors can still be quite large when the training data and holdout data come from one distribution and the unseen data comes from another. This is more akin to a domain gap. Both the PINN collision loss and the regularization obtained via the PCA model help to alleviate these issues with out-of-distribution unseen data. Even though the network-inferenced cloth may not follow the dynamic trajectory of the virtual bones as closely as one might prefer, the cloth tends to have an aesthetically pleasing shape and be interpenetration-free.

8 NEURAL SHAPE INFERENCE

Similar to the neural skinning in Section 7, we utilize a 2-layer MLP with 500 neurons per layer in order to inference about 100 PCA coefficients from the non-rigid displacements of the virtual bones from their positions in the cloth rest state. The same 5000 frames of simulated data is used for training; however, the PCA model is calculated based on the non-rigid displacement between the output of the neural skinning network and the ground truth (see [Wang and Lai 2024] for interesting discussion on multi-stage approaches). While the neural skinning is responsible for constructing a coarse approximation to the cloth mesh, the neural shape inference focuses on capturing more of the high-frequency spatial detail. This is obvious when comparing the two PCA models (See Figure 8). Similar to Section 7, a PINN-style collision loss is also included.

9 RESULTS AND DISCUSSION

For both the neural skinning and the neural shape networks, we used a weight of 0.1 on the data term and weight of 1000 on the PINN-style collision loss. The initial learning rate for Adam [Kingma and Ba 2014] was set to 10^{-4} to train the neural skinning network and 10^{-5} to train the neural shape network. A smaller learning rate was specified for the neural shape network, since its PCA coefficients represent smaller displacements. A cosine annealing schedule was used to decay the learning rate over epochs. The collision body SDFs were expanded by a small amount, and only one iteration was used for push out (for computational efficiency).

We obtained our 5000 frames of training data (for both the cape and the skirt) using Houdini Vellum. 80 percent of the frames were used in the loss function to train the neural network, and 10 percent of the frames (unseen in training) were used in a validation loss in order to choose parameters that might generalize well. Figures 9 and 10 demonstrate the efficacy of the neural skinning network and the neural shape network respectively. Another 10 percent of the frames were kept as true holdout data, in order to predict the ability of the networks to generalize to unseen (but still in-distribution) data. See Figure 11. Finally, Figure 12 showcases the efficacy of the PINN-style collision loss.

In order to demonstrate how our networks generalize to unseen out-of distribution data from rope chain simulations, we considered two types of loose-fitting garments: capes and skirts. See Figures 15 and 16. Weak lateral springs were added in order to connect virtual bones from different rope chains (for both the skirt and the cape). Wind drag was added to the cape virtual bones. Damping, relative to the parent virtual bone in the chain, was added to the skirt virtual bones. The rope chains were collided against the analytic SDFs depicted in Figure 6. Given the virtual bone positions obtained via rope chain simulation, we reconstructed the full cloth mesh using the neural skinning and neural shape networks. Even though the virtual bone positions generated from the rope chain simulations are out of distribution as compared to the training, validation, and holdout data, Figures 15 and 16 demonstrate that the networks generalized well and obtained good results.

Finally, we consider an RNN approach. Following the low frequency module in [Pan et al. 2022], we trained a Gated Recurrent Unit (GRU) [Cho et al. 2014]. The inputs are the current body pose and the latent vector from the prior state, and the outputs are the current virtual bone positions and the current latent vector. For the sake of a fair comparison, we used the same 5000 frames of (cape) simulation as training data; however, the RNN would obviously benefit from having access to an increased amount of training data. A separate RNN was trained for each rope chain. See Figures 13 and 14. Alternatively, the RNNs could be trained to match rope chain simulations; however, there is no reason to believe that predicting out-of-distribution data would fair any better than predicting in-distribution data.

10 CONCLUSION AND FUTURE WORK

We presented a novel method for the real-time simulation of loose-fitting garments leveraging neural networks for both skinning and shape inference. We demonstrated that only a small number of



Fig. 9. The first row shows the results of the neural skinning network, which can be compared to the ground truth training data in the second row. In order to demonstrate that the network does have the ability to match the ground truth data, the third row shows the overfit results obtained via overtraining; of course, an overfit network will not generalize well to unseen data.



Fig. 10. The first row shows the results of the neural skinning network (identical to the first row in Figure 9). The second row shows the results of the neural shape network applied on top of the neural skinning result. The third row shows the ground truth training data. The fourth row shows how overtraining the neural shape network leads to results that well match (albeit overfit, similar to the last row in Figure 9) the ground truth training data.

degrees of freedom is necessary in order to capture the ballistic motions. In order to overcome the locking artifacts typically incurred by using only a small number of degrees of freedom, we proposed a rope chain simulation method that maintains inextensibility while still allowing swinging, rotating, and buckling without resistance. A new history-based approach to collisions was introduced in order to accommodate fast-moving collision bodies and large time steps. A neural skinning solution was utilized in order to create a cloth mesh from the rope chain simulation degrees of freedom, and a quasistatic neural shape network was subsequently used in order



Fig. 11. The first row shows the results of the neural skinning network, and the second row shows the results of the neural shape network applied on top of the neural skinning result. These holdout frames from the training set give some indication of how the network will perform on unseen data. Note that the network needs to generalize to out-of-distribution data (from rope chain simulations, as is discussed in the last paragraph in Section 7), not just to holdout frames from the training set.

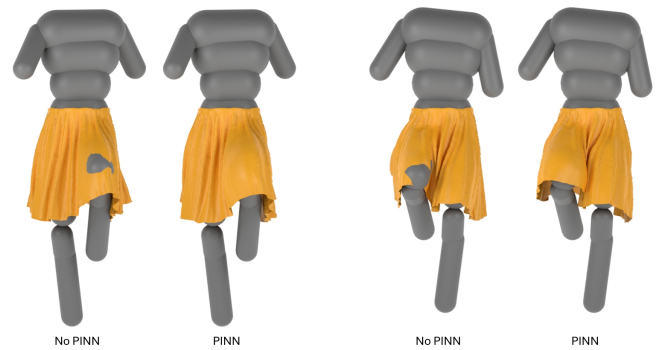


Fig. 12. Comparing the result of a neural skinning network trained without and with the PINN-style collision loss.

to add additional details. These networks were trained with the aid of a PINN-style collision loss.

Since they are based on the PCA coefficients, the neural skinning and shape networks produce reasonable mesh output even with out-of-distribution input; however, out-of-distribution input does adversely affect their ability to maintain an interpenetration-free state. Training the networks with a PINN-style collision loss gives reasonably penetration-free results for in-distribution data, but not necessarily for out-of-distribution data. Improving the interpenetration-freeness for out-of-distribution input is perhaps the most important area for the future work. Although the mesh could be post-processed to be interpenetration-free, doing so significantly decreases performance and thus the applicability for real-time applications. It is relatively cheap to process collisions for a small number of virtual bones, but far more expensive to process collisions for the entire mesh. Other interesting directions for future work include: making the rope chain simulation differentiable in order to automatically find constitutive parameters that best match the ground truth, investigating different network architectures for the neural skinning,

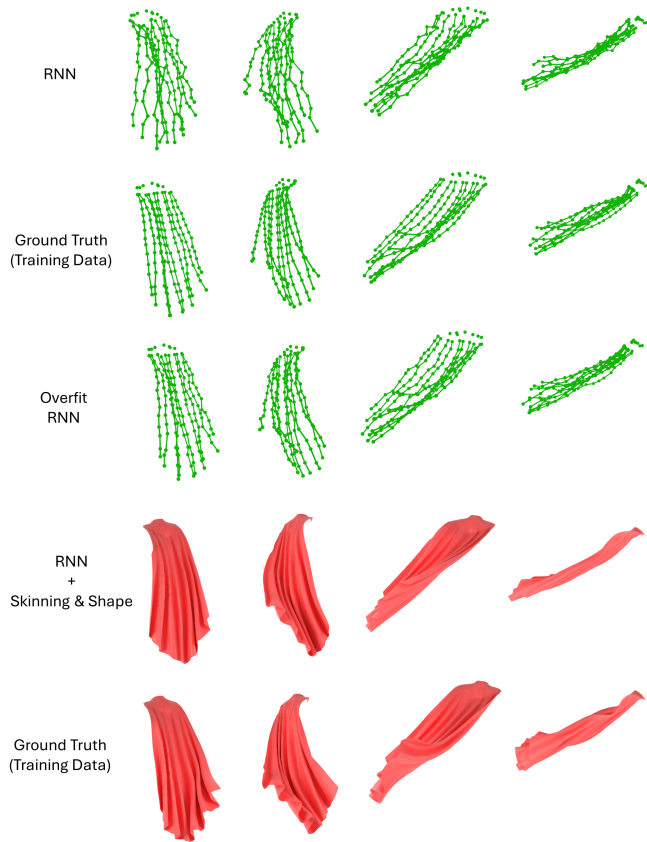


Fig. 13. We trained a separate RNN for each rope chain (10 RNNs in total). The RNN results (first row) are quite noisy compared to the ground truth training data (second row). The third row shows the overfit results obtained via overtraining. The fourth row shows the result of applying our neural skinning and neural shape inference to the RNN-inferred virtual bone positions (from the first row). Comparing these results to the ground truth training data (fifth row) illustrates that our networks generalize well to this noisy RNN input.

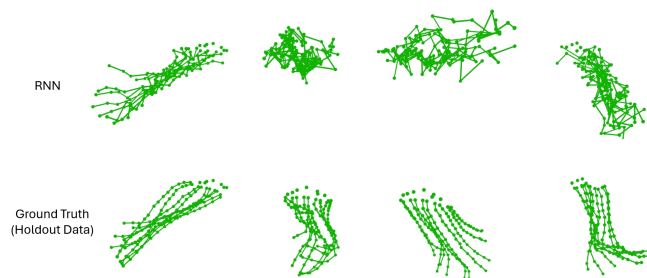


Fig. 14. The main issue with the RNN is that it generalizes very poorly to the holdout data. Presumably, this issue could be fixed by collecting more and more training data, but that excessively increases the cost incurred in both data collection (via numerical simulation) and training (via optimization). Even though our skinning and shape networks can smooth the noise in this RNN output (as they did in Figure 13), the dynamics will still be completely wrong.

generalizing a single network so that it can be used across different garment types and/or body shapes, etc.

ACKNOWLEDGMENTS

Research supported in part by ONR N00014-19-1-2285, ONR N00014-21-1-2771, Epic Games, and Sony. We would like to thank Reza and Behzad at ONR for supporting our efforts into machine learning. We would also like to thank Michael Lentine for various insightful discussions.

REFERENCES

- Dragomir Anguelov, Praveen Srinivasan, Daphne Koller, Sebastian Thrun, Jim Rodgers, and James Davis. 2005. Scape: shape completion and animation of people. In *ACM SIGGRAPH 2005 Papers*. 408–416.
- Stephen W Bailey, Dalton Omens, Paul Dilorenzo, and James F O’Brien. 2020. Fast and deep facial deformations. *ACM Transactions on Graphics (TOG)* 39, 4 (2020), 94–1.
- Stephen W Bailey, Dave Otte, Paul Dilorenzo, and James F O’Brien. 2018. Fast and deep deformation approximations. *ACM Transactions on Graphics (TOG)* 37, 4 (2018), 1–12.
- David Baraff and Andrew Witkin. 1998. Large steps in cloth simulation. In *Proceedings of the 25th annual conference on Computer graphics and interactive techniques*. 43–54.
- Hugo Bertiche, Meysam Madadi, and Sergio Escalera. 2021a. PBNS: physically based neural simulation for unsupervised garment pose space deformation. *ACM Trans. Graph.* 40, 6 (2021), 198:1–198:14. <https://doi.org/10.1145/3478513.3480479>
- Hugo Bertiche, Meysam Madadi, Emilio Tylson, and Sergio Escalera. 2021b. DeePSD: Automatic deep skinning and pose space deformation for 3D garment animation. In *Proceedings of the IEEE/CVF International Conference on Computer Vision*. 5471–5480.
- James F Blinn. 1982. A generalization of algebraic surface drawing. *ACM transactions on graphics (TOG)* 1, 3 (1982), 235–256.
- Robert Bridson, Ronald Fedkiw, and John Anderson. 2002. Robust treatment of collisions, contact and friction for cloth animation. In *Proceedings of the 29th annual conference on Computer graphics and interactive techniques*. 594–603.
- Robert Bridson, Sebastian Marino, and Ronald Fedkiw. 2003. Simulation of Clothing with Folds and Wrinkles. In *Proceedings of the 2003 ACM SIGGRAPH/Eurographics Symposium on Computer Animation (San Diego, California) (SCA '03)*. Eurographics Association, Goslar, DEU, 28–36.
- Nuttapong Chentanez, Miles Macklin, Matthias Müller, Stefan Jeschke, and Tae-Yong Kim. 2020. Cloth and skin deformation with a triangle mesh based convolutional neural network. In *Computer Graphics Forum*, Vol. 39. Wiley Online Library, 123–134.
- Kyunghyun Cho, Bart Van Merriënboer, Caglar Gulcehre, Dzmitry Bahdanau, Fethi Bougares, Holger Schwenk, and Yoshua Bengio. 2014. Learning phrase representations using RNN encoder-decoder for statistical machine translation. *arXiv preprint arXiv:1406.1078* (2014).
- Kwang-Jin Choi and Hyeong-Seok Ko. 2002. Stable but Responsive Cloth. *ACM Trans. Graph.* 21, 3 (July 2002), 604–611.
- Edilson De Aguiar, Leonid Sigal, Adrien Treuille, and Jessica K Hodgins. 2010. Stable spaces for real-time clothing. *ACM Transactions on Graphics (TOG)* 29, 4 (2010), 1–9.
- Junqi Diao, Jun Xiao, Yihong He, and Haiyong Jiang. 2023. Combating Spurious Correlations in Loose-fitting Garment Animation Through Joint-Specific Feature Learning. In *Computer Graphics Forum*, Vol. 42. Wiley Online Library, e14939.
- Lawson Fulton, Vismay Modi, David Duvinaud, David IW Levin, and Alec Jacobson. 2019. Latent-space dynamics for reduced deformable simulation. In *Computer graphics forum*, Vol. 38. Wiley Online Library, 379–391.
- Naga K Govindaraju, David Knott, Nitin Jain, Ilknur Kabul, Rasmus Tamstorf, Russell Gayle, Ming C Lin, and Dinesh Manocha. 2005. Interactive collision detection between deformable models using chromatic decomposition. *ACM Transactions on graphics (TOG)* 24, 3 (2005), 991–999.
- Artur Grigorev, Michael J Black, and Otmar Hilliges. 2023. HOOD: Hierarchical Graphs for Generalized Modelling of Clothing Dynamics. In *Proceedings of the IEEE/CVF Conference on Computer Vision and Pattern Recognition*. 16965–16974.
- Peng Guan, Loretta Reiss, David A Hirschberg, Alexander Weiss, and Michael J Black. 2012. Drape: Dressing any person. *ACM Transactions on Graphics (TOG)* 31, 4 (2012), 1–10.
- Eran Guendelman, Robert Bridson, and Ronald Fedkiw. 2003. Nonconvex rigid bodies with stacking. *ACM transactions on graphics (TOG)* 22, 3 (2003), 871–878.
- Erhan Gundogdu, Victor Constantin, Amrollah Seifoddini, Minh Dang, Mathieu Salzmann, and Pascal Fua. 2019. Garnet: A two-stream network for fast and accurate 3d cloth draping. In *Proceedings of the IEEE/CVF International Conference on Computer Vision*. 8739–8748.
- Fabian Hahn, Bernhard Thomaszewski, Stelian Coros, Robert W Sumner, Forrester Cole, Mark Meyer, Tony DeRose, and Markus Gross. 2014. Subspace clothing simulation



Fig. 15. Simulation of a cape on an animation of a running person. First row: rope chain simulation. The rope chains are shaded green, and the weak lateral springs are visualized as purple edges. Second row: neural skinning, based on the first row. Third row: neural shape inference, based on the second row. Fourth row: Houdini cloth simulation with approximately 12K vertices (as a reference). The Houdini simulation and our rope chain approach both produce good dynamics, although the Houdini simulation does exhibit visually displeasing erroneous over-stretching artifacts; in addition, the Houdini simulation is an order of magnitude slower than our currently unoptimized code.

- using adaptive bases. *ACM Transactions on Graphics (TOG)* 33, 4 (2014), 1–9.
- Daniel Holden, Bang Chi Duong, Sayantan Datta, and Derek Nowrouzezahrai. 2019. Subspace neural physics: Fast data-driven interactive simulation. In *Proceedings of the 18th annual ACM SIGGRAPH/Eurographics Symposium on Computer Animation*. 1–12.
- Ning Jin, Wenlong Lu, Zhenglin Geng, and Ronald P Fedkiw. 2017. Inequality cloth. In *Proceedings of the ACM SIGGRAPH/Eurographics symposium on computer animation*. 1–10.
- Ning Jin, Yilin Zhu, Zhenglin Geng, and Ronald Fedkiw. 2020. A pixel-based framework for data-driven clothing. In *Computer Graphics Forum*, Vol. 39. Wiley Online Library, 135–144.
- Yongxu Jin, Yushan Han, Zhenglin Geng, Joseph Teran, and Ronald Fedkiw. 2022. Analytically Integratable Zero-restlength Springs for Capturing Dynamic Modes unrepresented by Quasistatic Neural Networks. In *ACM SIGGRAPH 2022 Conference Proceedings*. 1–9.
- Ladislav Kavan, Steven Collins, Jiří Žára, and Carol O’Sullivan. 2007. Skinning with dual quaternions. In *Proceedings of the 2007 symposium on Interactive 3D graphics and games*. 39–46.
- Ladislav Kavan, Steven Collins, Jiří Žára, and Carol O’Sullivan. 2008. Geometric skinning with approximate dual quaternion blending. *ACM Transactions on Graphics (TOG)* 27, 4 (2008), 1–23.
- Ladislav Kavan, Dan Gerszewski, Adam W Bargteil, and Peter-Pike Sloan. 2011. Physics-inspired upsampling for cloth simulation in games. In *ACM SIGGRAPH 2011 papers*. 1–10.
- Doyub Kim, Woojong Koh, Rahul Narain, Kayvon Fatahalian, Adrien Treuille, and James F O’Brien. 2013. Near-exhaustive precomputation of secondary cloth effects. *ACM Transactions on Graphics (TOG)* 32, 4 (2013), 1–8.
- Diederik P Kingma and Jimmy Ba. 2014. Adam: A method for stochastic optimization. *arXiv preprint arXiv:1412.6980* (2014).
- Tsuneya Kurihara and Natsuki Miyata. 2004. Modeling deformable human hands from medical images. In *Proceedings of the 2004 ACM SIGGRAPH/Eurographics symposium*

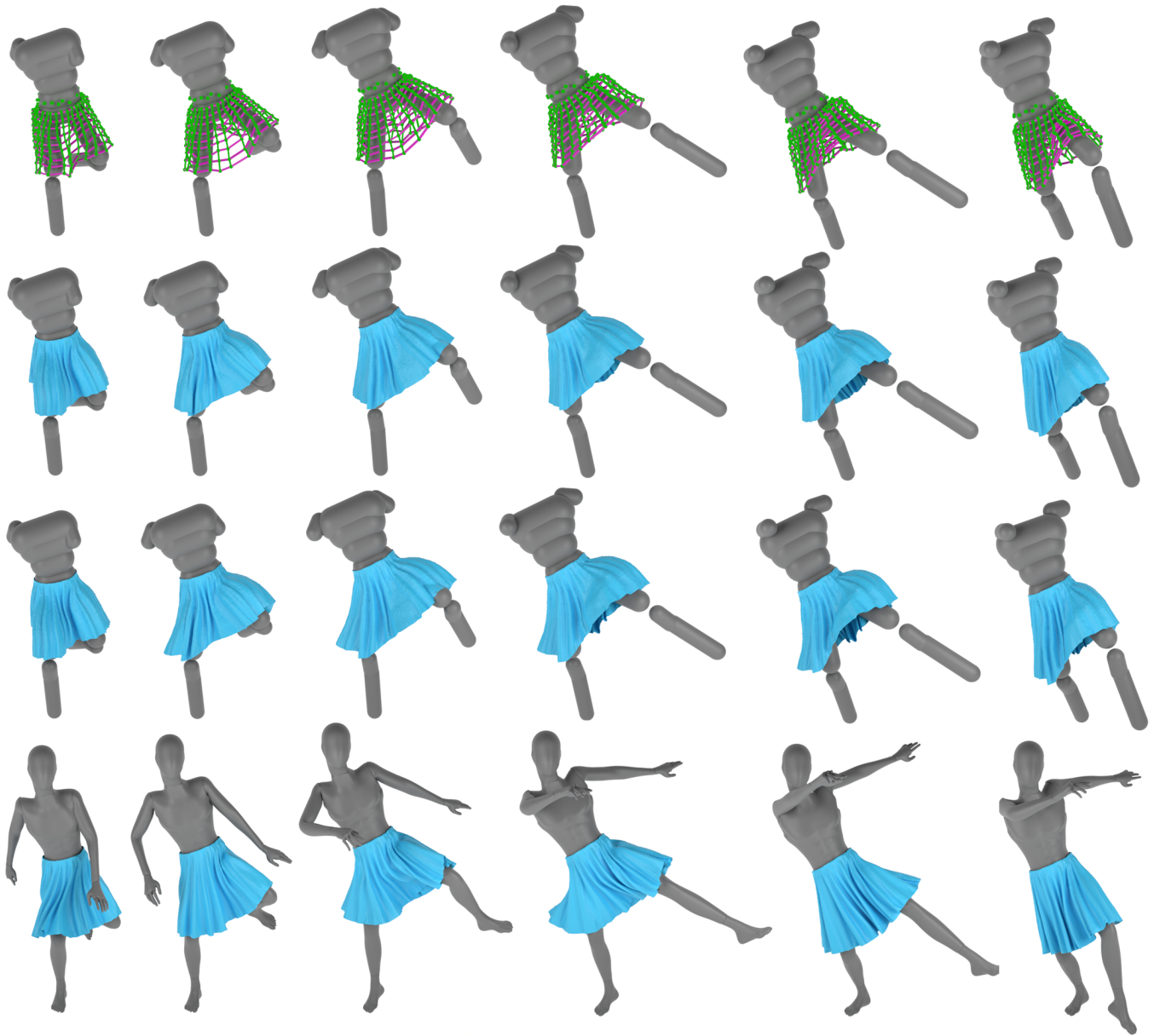


Fig. 16. Simulation of a skirt on an animation of a dancing person. First row: rope chain simulation. The rope chains are shaded green, and the weak lateral springs are visualized as purple edges. Second row: neural skinning, based on the first row. Third row: neural shape inference, based on the second row. Fourth row: Houdini cloth simulation with approximately 18K vertices (as a reference). The skirt is rendered with a blue color in order to differentiate it from the yellow skirt figures, which use barycentrically embedded virtual bone positions instead of rope chain simulations as the network input.

on *Computer animation*. 355–363.
 Zorah Lahner, Daniel Cremers, and Tony Tung. 2018. Deepwrinkles: Accurate and realistic clothing modeling. In *Proceedings of the European conference on computer vision (ECCV)*. 667–684.
 Binh Huy Le and Zhigang Deng. 2012. Smooth skinning decomposition with rigid bones. *ACM Transactions on Graphics (TOG)* 31, 6 (2012), 1–10.
 Dohaee Lee, Hyun Kang, and In-Kwon Lee. 2023. ClothCombo: Modeling Inter-Cloth Interaction for Draping Multi-Layered Clothes. *ACM Transactions on Graphics (TOG)* 42, 6 (2023), 1–13.

Christopher Lewin. 2021. Swish: Neural Network Cloth Simulation on Madden NFL 21. In *ACM SIGGRAPH 2021 Talks*. 1–2.
 John P Lewis, Matt Cordner, and Nickso Fong. 2000. Pose space deformation: a unified approach to shape interpolation and skeleton-driven deformation. In *Proceedings of the 27th annual conference on Computer graphics and interactive techniques 2000*. ACM Press/Addison-Wesley Publishing Co., 165–172.
 Cheng Li, Min Tang, Ruofeng Tong, Ming Cai, Jieyi Zhao, and Dinesh Manocha. 2020. P-cloth: interactive complex cloth simulation on multi-GPU systems using dynamic matrix assembly and pipelined implicit integrators. *ACM Transactions on Graphics (TOG)* 39, 6 (2020), 1–15.

- Ren Li, Benoît Guillard, and Pascal Fua. 2024. Isp: Multi-layered garment draping with implicit sewing patterns. *Advances in Neural Information Processing Systems* 36 (2024).
- Yu Di Li, Min Tang, Xiao Rui Chen, Yun Yang, Ruo Feng Tong, Bai Lin An, Shuang Cai Yang, Yao Li, and Qi Long Kou. 2023. D-Cloth: Skinning-based Cloth Dynamic Prediction with a Three-stage Network. In *Computer Graphics Forum*, Vol. 42. Wiley Online Library, e14937.
- Yu Di Li, Min Tang, Yun Yang, Zi Huang, Ruo Feng Tong, Shuang Cai Yang, Yao Li, and Dinesh Manocha. 2022. N-Cloth: Predicting 3D Cloth Deformation with Mesh-Based Networks. In *Computer Graphics Forum*, Vol. 41. Wiley Online Library, 547–558.
- Matthew Loper, Naureen Mahmood, Javier Romero, Gerard Pons-Moll, and Michael J. Black. 2015. SMPL: a skinned multi-person linear model. *ACM Trans. Graph.* 34, 6, Article 248 (oct 2015), 16 pages. <https://doi.org/10.1145/2816795.2818013>
- Ran Luo, Tianjia Shao, Huamin Wang, Weiwei Xu, Xiang Chen, Kun Zhou, and Yin Yang. 2018. NNWarp: Neural network-based nonlinear deformation. *IEEE transactions on visualization and computer graphics* 26, 4 (2018), 1745–1759.
- Thalmann Magnenat, Richard Laperrière, and Daniel Thalmann. 1988. *Joint-dependent local deformations for hand animation and object grasping*. Technical Report. Canadian Inf. Process. Soc.
- Ishit Mehta, Manmohan Chandraker, and Ravi Ramamoorthi. 2022. A level set theory for neural implicit evolution under explicit flows. In *European Conference on Computer Vision*. Springer, 711–729.
- Mathias Müller, Bruno Heidelberger, Marcus Hennix, and John Ratcliff. 2007. Position based dynamics. *Journal of Visual Communication and Image Representation* 18, 2 (2007), 109–118.
- Hitoshi Nishimura, Makoto Hirai, Toshiyuki Kawai, Toru Kawata, Isao Shirakawa, and Koichi Omura. 1985. Object modeling by distribution function and a method of image generation. *Journal of papers IEICE Japan* '85 68, 4 (1985).
- Young Jin Oh, Tae Min Lee, and In-Kwon Lee. 2018. Hierarchical cloth simulation using deep neural networks. In *Proceedings of Computer Graphics International 2018*. 139–146.
- Xiaoyu Pan, Jiaming Mai, Xinwei Jiang, Dongxue Tang, Jingxiang Li, Tianjia Shao, Kun Zhou, Xiaogang Jin, and Dinesh Manocha. 2022. Predicting loose-fitting garment deformations using bone-driven motion networks. In *ACM SIGGRAPH 2022 Conference Proceedings*. 1–10.
- Jeong Joon Park, Peter Florence, Julian Straub, Richard Newcombe, and Steven Lovegrove. 2019. DeepSDF: Learning continuous signed distance functions for shape representation. In *Proceedings of the IEEE/CVF conference on computer vision and pattern recognition*. 165–174.
- Chaitanya Patel, Zhouyingcheng Liao, and Gerard Pons-Moll. 2020. Tailornet: Predicting clothing in 3d as a function of human pose, shape and garment style. In *Proceedings of the IEEE/CVF Conference on Computer Vision and Pattern Recognition*. 7365–7375.
- Tobias Pfaff, Meire Fortunato, Alvaro Sanchez-Gonzalez, and Peter W. Battaglia. 2021. Learning Mesh-Based Simulation with Graph Networks. In *9th International Conference on Learning Representations, ICLR 2021, Virtual Event, Austria, May 3-7, 2021*.
- Gerard Pons-Moll, Javier Romero, Naureen Mahmood, and Michael J Black. 2015. Dyna: A model of dynamic human shape in motion. *ACM Transactions on Graphics (TOG)* 34, 4 (2015), 1–14.
- Xavier Provot. 1997. Collision and self-collision handling in cloth model dedicated to design garments. In *Computer Animation and Simulation '97: Proceedings of the Eurographics Workshop in Budapest, Hungary, September 2-3, 1997*. Springer, 177–189.
- Maziar Raissi, Paris Perdikaris, and George E Karniadakis. 2019. Physics-informed neural networks: A deep learning framework for solving forward and inverse problems involving nonlinear partial differential equations. *Journal of Computational physics* 378 (2019), 686–707.
- Edoardo Remelli, Artem Lukoianov, Stephan Richter, Benoît Guillard, Timur Bagautdinov, Pierre Baque, and Pascal Fua. 2020. MeshSDF: Differentiable iso-surface extraction. *Advances in Neural Information Processing Systems* 33 (2020), 22468–22478.
- Nadine Abu Ruman and Marco Fratarcangeli. 2017. Skin Deformation Methods for Interactive Character Animation. In *Computer Vision, Imaging and Computer Graphics Theory and Applications: 11th International Joint Conference, VISIGRAPP 2016, Rome, Italy, February 27-29, 2016, Revised Selected Papers 11*. Springer, 153–174.
- Shunsuke Saito, Zeng Huang, Ryota Natsume, Shigeo Morishima, Angjoo Kanazawa, and Hao Li. 2019. Pifu: Pixel-aligned implicit function for high-resolution clothed human digitization. In *Proceedings of the IEEE/CVF international conference on computer vision*. 2304–2314.
- Alvaro Sanchez-Gonzalez, Jonathan Godwin, Tobias Pfaff, Rex Ying, Jure Leskovec, and Peter Battaglia. 2020. Learning to simulate complex physics with graph networks. In *International conference on machine learning*. PMLR, 8459–8468.
- Igor Santesteban, Miguel A Otaduy, and Dan Casas. 2019. Learning-based animation of clothing for virtual try-on. In *Computer Graphics Forum*, Vol. 38. Wiley Online Library, 355–366.
- Igor Santesteban, Miguel A Otaduy, and Dan Casas. 2022. SNUG: Self-Supervised Neural Dynamic Garments. *IEEE/CVF Conference on Computer Vision and Pattern Recognition (CVPR)* (2022).
- Igor Santesteban, Nils Thuerey, Miguel A Otaduy, and Dan Casas. 2021. Self-supervised collision handling via generative 3d garment models for virtual try-on. In *Proceedings of the IEEE/CVF Conference on Computer Vision and Pattern Recognition*. 11763–11773.
- Andrew Selle, Jonathan Su, Geoffrey Irving, and Ronald Fedkiw. 2008. Robust high-resolution cloth using parallelism, history-based collisions, and accurate friction. *IEEE transactions on visualization and computer graphics* 15, 2 (2008), 339–350.
- Yidi Shao, Chen Change Loy, and Bo Dai. 2023. Towards Multi-Layered 3D Garments Animation. In *Proceedings of the IEEE/CVF International Conference on Computer Vision*. 14361–14370.
- Tianchang Shen, Jun Gao, Kangxue Yin, Ming-Yu Liu, and Sanja Fidler. 2021. Deep marching tetrahedra: a hybrid representation for high-resolution 3d shape synthesis. *Advances in Neural Information Processing Systems* 34 (2021), 6087–6101.
- Avneesh Sud, Naga Govindaraju, Russell Gayle, Ilknur Kabul, and Dinesh Manocha. 2006. Fast proximity computation among deformable models using discrete voronoi diagrams. In *ACM SIGGRAPH 2006 Papers*. 1144–1153.
- Qingyang Tan, Zherong Pan, Lin Gao, and Dinesh Manocha. 2020. Realtime simulation of thin-shell deformable materials using CNN-based mesh embedding. *IEEE Robotics and Automation Letters* 5, 2 (2020), 2325–2332.
- Qingyang Tan, Yi Zhou, Tuanfeng Wang, Duygu Ceylan, Xin Sun, and Dinesh Manocha. 2022. A Repulsive Force Unit for Garment Collision Handling in Neural Networks. In *European Conference on Computer Vision*. Springer, 451–467.
- Min Tang, Ruofeng Tong, Zhendong Wang, and Dinesh Manocha. 2014. Fast and exact continuous collision detection with bernstein sign classification. *ACM Transactions on Graphics (TOG)* 33, 6 (2014), 1–8.
- Min Tang, Tongtong Wang, Zhongyuan Liu, Ruofeng Tong, and Dinesh Manocha. 2018. I-Cloth: Incremental collision handling for GPU-based interactive cloth simulation. *ACM Transactions on Graphics (TOG)* 37, 6 (2018), 1–10.
- Demetri Terzopoulos, John Platt, Alan Barr, and Kurt Fleischer. 1987. Elastically deformable models. In *Proceedings of the 14th annual conference on Computer graphics and interactive techniques*. 205–214.
- Huamin Wang, Florian Hecht, Ravi Ramamoorthi, and James F O'Brien. 2010. Example-based wrinkle synthesis for clothing animation. In *ACM SIGGRAPH 2010 papers*. 1–8.
- Tuanfeng Y Wang, Tianjia Shao, Kai Fu, and Niloy J Mitra. 2019. Learning an intrinsic garment space for interactive authoring of garment animation. *ACM Transactions on Graphics (TOG)* 38, 6 (2019), 1–12.
- Yongji Wang and Ching-Yao Lai. 2024. Multi-stage neural networks: Function approximator of machine precision. *J. Comput. Phys.* (2024), 112865.
- Jane Wu, Diego Thomas, and Ronald Fedkiw. 2023. Weakly-Supervised 3D Reconstruction of Clothed Humans via Normal Maps. *arXiv preprint arXiv:2311.16042* (2023).
- Geoff Wyvill, Craig McPheeters, and Brian Wyvill. 1986. Soft objects. In *Advanced Computer Graphics: Proceedings of Computer Graphics Tokyo'86*. Springer, 113–128.
- Weiwei Xu, Nobuyuki Umetani, Qianwen Chao, Jie Mao, Xiaogang Jin, and Xin Tong. 2014. Sensitivity-optimized rigging for example-based real-time clothing synthesis. *ACM Trans. Graph.* 33, 4 (2014), 107–1.
- Meng Zhang, Tuanfeng Y Wang, Duygu Ceylan, and Niloy J Mitra. 2021. Dynamic neural garments. *ACM Transactions on Graphics (TOG)* 40, 6 (2021), 1–15.
- Fang Zhao, Zekun Li, Shaoli Huang, Junwu Weng, Tianfei Zhou, Guo-Sen Xie, Jue Wang, and Ying Shan. 2023. Learning Anchor Transformations for 3D Garment Animation. In *Proceedings of the IEEE/CVF Conference on Computer Vision and Pattern Recognition*. 491–500.
- Mianlun Zheng, Yi Zhou, Duygu Ceylan, and Jernej Barbic. 2021. A deep emulator for secondary motion of 3d characters. In *Proceedings of the IEEE/CVF Conference on Computer Vision and Pattern Recognition*. 5932–5940.